

UNIVERSIDADE ESTADUAL DE CAMPINAS
SISTEMA DE BIBLIOTECAS DA UNICAMP
REPOSITÓRIO DA PRODUÇÃO CIENTÍFICA E INTELECTUAL DA UNICAMP

Versão do arquivo anexado / Version of attached file:

Versão do Editor / Published Version

Mais informações no site da editora / Further information on publisher's website:

<https://www.mdpi.com/2304-6740/11/8/331>

DOI: <https://doi.org/10.3390/inorganics11080331>

Direitos autorais / Publisher's copyright statement:

©2023 by MDPI. All rights reserved.

DIRETORIA DE TRATAMENTO DA INFORMAÇÃO

Cidade Universitária Zeferino Vaz Barão Geraldo






CEP 13083-970 – Campinas SP

Fone: (19) 3521-6493

<http://www.repositorio.unicamp.br>

Article

Copper(II) and Platinum(II) Naproxenates: Insights on Synthesis, Characterization and Evaluation of Their Antiproliferative Activities

Amanda A. Silva ¹, Silmara C. L. Frajácómo ², Álefe B. Cruz ³, Kaio Eduardo Buglio ⁴, Daniele Daiane Affonso ⁴ , Marcelo Cecconi Portes ⁵ , Ana Lúcia T. G. Ruiz ⁴ , João Ernesto de Carvalho ⁴, Wilton R. Lustri ², Douglas H. Pereira ³ , Ana M. da Costa Ferreira ⁵  and Pedro P. Corbi ^{1,*}

¹ Institute of Chemistry, University of Campinas—UNICAMP, Campinas 13083-970, SP, Brazil; a265988@dac.unicamp.br

² Department of Biological and Health Sciences, University of Araraquara—UNIARA, Araraquara 14801-320, SP, Brazil; scfajacom@uniara.edu.br (S.C.L.F.); wrlustri@uniara.edu.br (W.R.L.)

³ Chemistry Collegiate, Federal University of Tocantins—UFT, Gurupi 77402-970, TO, Brazil; allefe.cruz@uft.edu.br (Á.B.C.); doug@mail.uft.edu.br (D.H.P.)

⁴ Faculty of Pharmaceutical Sciences, University of Campinas-UNICAMP, Campinas 13083-871, SP, Brazil; kaiobuglio@gmail.com (K.E.B.); ana.ruiz@fcf.unicamp.br (A.L.T.G.R.); carvalho@fcf.unicamp.br (J.E.d.C.)

⁵ Department of Fundamental Chemistry, Institute of Chemistry, University of São Paulo—USP, São Paulo 05508-000, SP, Brazil; marcelo_cecconi@hotmail.com (M.C.P.); amdcferr@iq.usp.br (A.M.d.C.F.)

* Correspondence: ppcorbi@unicamp.br

Abstract: The growth of antibiotic resistance is a matter of worldwide concern. In parallel, cancer remains one of the main causes of death. In the search for new and improved antiproliferative agents, one of the strategies is the combination of bioactive ligands and metals that are already consolidated in the synthesis of metallopharmaceutical agents. Thus, this work deals with the synthesis, characterization, and study of naproxen (Nap)-based complexes of copper(II) and platinum(II) as antiproliferative agents. The copper complex (Cu–Nap) presents a binuclear paddle-wheel structure in a 1 Cu:2 Nap:1 H₂O molar composition, in which Cu(II) is bonded to the carboxylate oxygens from naproxenate in a bidentate bridging mode. The platinum complex (Pt–Nap) was identified as the square planar *cis*-[Pt(Nap)₂(DMSO)₂] isomer, in which Pt(II) is bonded to the carboxylate oxygen atom of Nap in a monodentate fashion. Both complexes were inactive against the Gram-positive and Gram-negative bacterial strains assessed. Pt–Nap presented low cytostatic behavior over a set of tumor cells, but good viability for normal cells, while Cu–Nap was cytotoxic against all cells, with a cytotoxic activity against glioma tumor cells.

Keywords: NSAIDs; copper(II); platinum(II); naproxen; antibacterial agents; antiproliferative activities



Citation: Silva, A.A.; Frajácómo, S.C.L.; Cruz, Á.B.; Buglio, K.E.; Affonso, D.D.; Portes, M.C.; Ruiz, A.L.T.G.; de Carvalho, J.E.; Lustri, W.R.; Pereira, D.H.; et al. Copper(II) and Platinum(II) Naproxenates: Insights on Synthesis, Characterization and Evaluation of Their Antiproliferative Activities. *Inorganics* **2023**, *11*, 331. <https://doi.org/10.3390/inorganics11080331>

Academic Editor: Vladimir Arion

Received: 13 July 2023

Revised: 7 August 2023

Accepted: 7 August 2023

Published: 10 August 2023



Copyright: © 2023 by the authors. Licensee MDPI, Basel, Switzerland. This article is an open access article distributed under the terms and conditions of the Creative Commons Attribution (CC BY) license (<https://creativecommons.org/licenses/by/4.0/>).

1. Introduction

An intense search for new broad-spectrum antimicrobial agents active against multidrug-resistant bacterial strains has been carried out worldwide. The misuse of antibiotics, not only in humans but also in livestock and agriculture, either to prevent or cure diseases led to microbial resistance and chronic infections. This situation not only caused the deaths of millions of people around the world, but also impacted the financial systems of many countries [1]. Furthermore, the search for new pharmacologically active agents in tumor cells, with improved activities and reduced adverse reactions, is necessary. By 2025, more than 20 million new cases of cancer are expected each year, requiring the development of new drug treatments and personalized therapies [1,2].

To overcome these two major challenges in current medicine, the preparation of bioactive coordination compounds with metals is considered a promising strategy. For a review,

see Štarha and Trávníček [3]. In the 1960s, a new era of development of drugs containing metals began, with the discovery of the inhibitory activities of cisplatin on the proliferation of *Escherichia coli* strains and different tumor cell lines [2,4]. Today, cisplatin and its derivatives, carboplatin and oxaliplatin, are widely used in clinics as chemotherapeutics for ovarian, testicular, and melanoma cancers, among others [5]. However, resistance, combined with poor selectivity, has become an issue in therapy with platinum drugs. Additionally, high doses of the drugs became necessary to ensure that the exact concentration of Pt(II) reached the intracellular medium. This practice can lead to adverse effects, such as nephrotoxicity, neurotoxicity, ototoxicity, and gastrointestinal reactions, which can, in turn, lead to interruption of cancer treatment [5–7].

Thus, the search for alternative metals, combined with bioactive ligands, has risen in recent decades. A typical example is silver sulfadiazine, which has been used since the 1970s in the treatment of bacterial infections [8]. Metal complexes have unique advantages, such as their redox properties and their own reaction mechanisms [9,10], and their biological properties [11–13]. A wide variety of ligands can be used, and some drugs already used in clinics can be associated with metals. Both cancer and bacterial infections promote an inflammatory response in the body. Thus, associating anti-inflammatories with metals with known biological activities seems to be an effective proposal. The combination of antibiotics with anti-inflammatories is already a widespread practice (polytherapy). Inhibitors of COXs, and possibly of MMPs as well—such as non-steroidal anti-inflammatory drugs (NSAIDs)—have been studied for the treatment of cancer [6,14,15].

Several mononuclear-, binuclear, and trinuclear Cu(II) complexes, in combination with NSAIDs such as mefenamic acid, diclofenac, diflunisal, indomethacin, aspirin, and naproxen, among others, are reported in the literature [9,16,17]. Some of these complexes showed better biological activities in vitro than their parental molecules. A recently synthesized Cu(II)-nimesulide complex, for example, presented a minimum inhibitory concentration (MIC) of 3.0 mmol L^{-1} against *Staphylococcus aureus* and 1.5 mmol L^{-1} against *Escherichia coli* and *Pseudomonas aeruginosa*, while nimesulide alone did not have antibacterial potential [18]. In addition, several platinum(IV) prodrugs with NSAIDs were reported by Spector et al. [19], Tolan et al. [20], and Chen et al. [15], and many of them presented higher antiproliferative activity in vitro than that of pure cisplatin.

Naproxen (Nap), (+)-(S)-2-(6-methoxynaphthalen-2-yl)propanoic acid, is an antipyretic and analgesic NSAID. It is widely used in the treatment of arthritis, spondylitis, bursitis, gout, and chronic pain [12,21]. Compared to other NSAIDs, it has shown less unwanted cardiovascular and nephron side effects [15]. It is a COX 1 and COX 2 inhibitor, and has shown inhibitory activity over MMPs, especially when associated with Pt(IV). Naproxen reduced carcinogenesis and proliferation of prostate, colon, and bladder tumor cells [15,17].

A great number of articles on naproxenate-based complexes, proving that these compounds may present useful biological activities, can be found in the literature. Studies related to the synthesis of metal complexes and their anti-inflammatory, antioxidant, and antiproliferative activities were reported [15,22]. In the literature, zinc, cobalt, copper, and iron complexes with naproxen have also been reported [23–25]. In particular, three binuclear copper(II) naproxenate complexes call attention to a paddle-wheel type coordination. The structures of $[\text{Cu}_2\text{L}_4(\text{H}_2\text{O})_2]$ complexes were proposed for the ligands (L) as the NSAIDs diclofenac, ibuprofen, and naproxen, based on infrared (IR) and Raman spectroscopic analysis and the crystal structure for the diclofenac complex [26]. In another study, the $[\text{Cu}_2(\text{Nap})_4(\text{H}_2\text{O})_2]$ presented good binding affinity to bovine serum albumin (BSA) and, especially, to human serum albumin (HSA) proteins, which take part in the transport of the metal complexes through the blood stream [27]. A $[\text{Cu}_2(\text{Nap})_4(\text{DMSO})_2]$ complex that presented antitumor properties loaded to chitosan beads was characterized, and this system showed a controlled release in gastric and intestinal pH [28]. Additionally, the monomeric Cu(II) complex $[\text{Cu}(\text{Nap})_2(\text{H}_2\text{O})_3](\text{H}_2\text{O})$ presented a higher anti-inflammatory response and a lower gastric ulcer than those of free naproxen, acting as urease inhibitors [23].

Still, most reports of naproxen-based complexes are compounds with various 3d transition metals (e.g., Co [21], Cu [23,29], and Zn [30]) associated to nitrogen donor heterocyclic ligands (1,10-phenanthroline, pyridine, and 2,2'-bipyridine, among others). They have been reported as antibacterial [12] or antitumoral agents [31], maintaining the anti-inflammatory and antioxidant properties.

In this context, other metals such as Pt(II) [7,32], Pd(II) [7], and Ru(II) [31] have also been combined with naproxen and nitrogen-donor ligands. Pt(II) naproxenate complexes with ethylenediamine and diaminocyclohexane presented selective antiproliferative activity against epithelial (MCF7) and human cervical carcinoma cells (HeLa), respectively [32,33].

This work expands upon the studies on the synthesis and spectroscopic characterizations of Cu(II) and Pt(II) complexes with naproxen, and also explores the antiproliferative activities of the complexes over pathogenic bacterial strains and tumor cells, seeking new drug candidates. A combination of experimental and theoretical (DFT) data were applied to propose the most probable structural formulae for the complexes.

2. Results

2.1. Infrared and Raman Spectroscopic Measurements

The main bands on the ATR-FTIR spectra of Cu-Nap, Pt-Nap and NaNap are presented in Figure 1. As a complement, the Raman spectra of Cu-Nap, Pt-Nap, NaNap, and *cis*-[PtCl₂(DMSO)₂] are presented in Figure 2. The far-IR spectra from 100–500 cm^{−1} of Cu-Nap and Pt-Nap are presented in Supplementary Figure S1 (Supplementary Materials). In the FTIR spectra, the main absorption bands of NaNap and attributions were at 3564–3143 cm^{−1} (νOH, broad band), 3057–2830 cm^{−1} (νCH), 1585 cm^{−1} (νCOO_{asym}), and 1390 cm^{−1} (νCOO_{sym}), which were in good agreement with the literature [26]. Meanwhile, the Cu-Nap FTIR spectrum presented a sharp strong band at 3601 cm^{−1} (νOH), instead of the broad band observed for NaNap. Other main signals (in cm^{−1}) for Cu-Nap were 3064–2800 (νCH), 1554 (νCOO_{asym}), and 1403 cm^{−1} (νCOO_{sym}). Thus, the difference between the νCOO asymmetric and symmetric stretchings Δ(νCOO_{asym} – νCOO_{sym}) for the Cu-Nap was 151 cm^{−1}, whereas for the free ligand the difference was 195 cm^{−1}. The weak signals from 100–600 cm^{−1} occurred for Cu–O stretching [27,34]. The broad medium intensity band with a maximum at ~1670 cm^{−1} may be assigned to the bending mode δ (HOH) of the coordination water molecule in the complex.

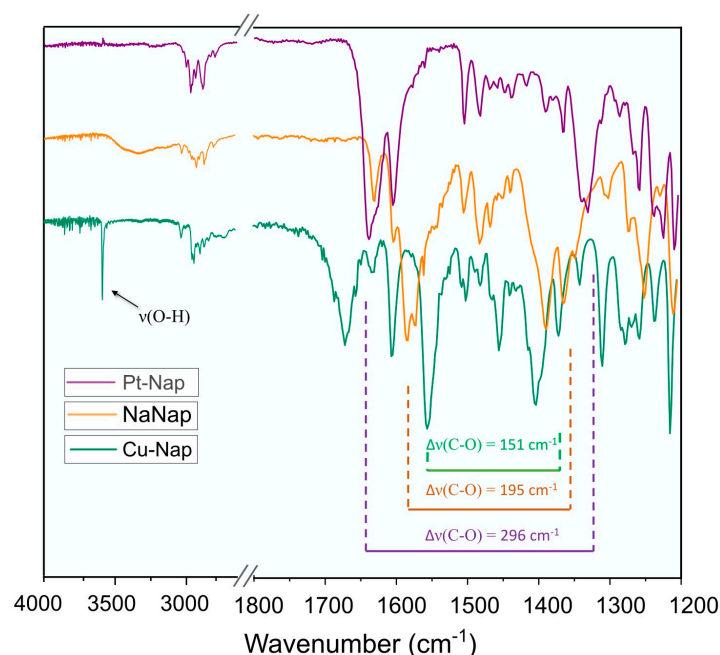


Figure 1. ATR-FTIR spectra of NaNap, Cu-Nap, and Pt-Nap (recorded from 4000 to 400 cm^{−1}) and identification of main bands.

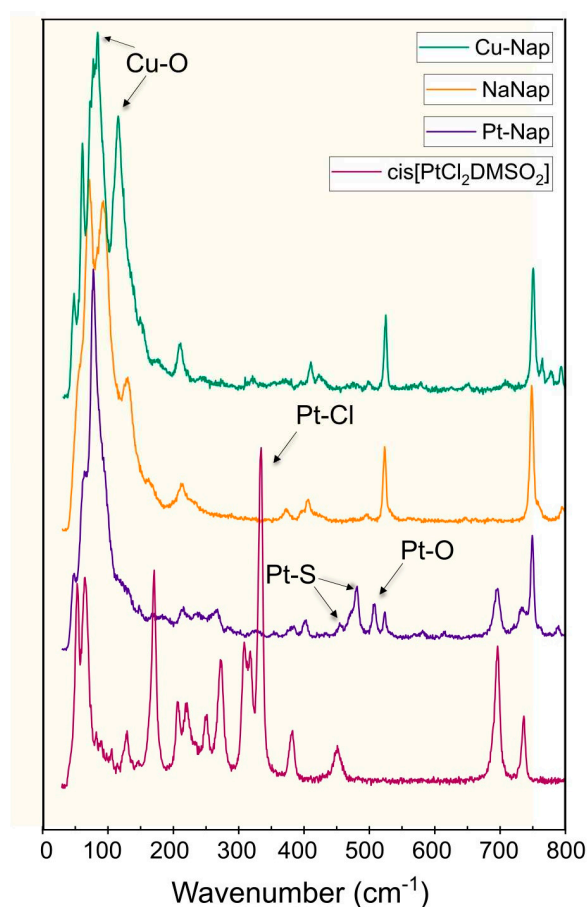


Figure 2. Raman spectra of the Cu-Nap and Pt-Nap complexes and their starting materials NaNap and $\text{cis-[PtCl}_2(\text{DMSO})_2]$.

Pt-Nap, for instance, showed FTIR bands for the respective wavenumbers (in cm^{-1}), as follows: 3064–2821 (νCH), 1637 ($\nu\text{COO}_{\text{asym}}$), and 1341 ($\nu\text{COO}_{\text{sym}}$). Thus, a Δ value of 296 cm^{-1} for Pt-Nap was observed. Additionally, a band and a shoulder were seen at 1144/1129 cm^{-1} , as shown in Supplementary Figure S2 in the Supplementary Materials. It corresponds to sulfoxide (νSO) stretching from DMSO. This result matches the one reported for $\text{cis-[PtCl}_2(\text{DMSO})_2]$ in the literature, attesting to the presence of DMSO in the structure in a *cis*-configuration [35]. In the Raman spectrum the Pt-S (Pt-DMSO), vibration was confirmed by the presence of a band and a shoulder at 480 cm^{-1} and 452 cm^{-1} , respectively, which also appeared for $\text{cis-[PtCl}_2(\text{DMSO})_2]$. In the far-FTIR of Pt-Nap, it was also possible to see the Pt-S stretching at 453/430 (Figure S1) [35]. The Pt-O stretching at 523 cm^{-1} in Raman was also seen, as well as in the FTIR spectrum of Pt-Nap [36]. However, it was not seen in Pt-Nap the Pt-Cl stretch identified for the precursor in Raman at 349 cm^{-1} , proving the substitution of both chlorides. Furthermore, the absence of a broad band of around 3400–3600 cm^{-1} in the IR spectrum of Pt-Nap indicated the absence of hydration water in its composition.

2.2. UV-Vis Spectroscopic Analysis and Kinetic Studies for the Cu-Nap Complex

The UV-Vis spectrum of Cu-Nap exhibited three absorption bands at 240 nm (seen only in chloroform), 260 nm, and 320 nm (chloroform and dimethylsulfoxide, respectively), which may be attributed to intraligand transitions. For Cu-Nap, a band in the visible region with its maximum at 715 nm was also observed and was attributed to d-d transitions. This band was in accordance with the obtained results obtained by Dimiza et al. [27] for a paddle-wheel copper(II) complex with naproxenate, as previously described, which was obtained in this work by a different synthetic method. While Cu-Nap is reported to retain

structure in either solid form or in solution [27], it was observed that, in DMSO, there was a minor change in the absorbance behavior throughout 24 h, indicating some solvent exchange. This is seen in Supplementary Figure S3, especially for the absorbance peaks of 260 nm and 275 nm during the first eight hours.

2.3. TGA Measurements

The TG/DTA thermograms of Cu–Nap and Pt–Nap are shown in Figure 3a,b, respectively. For Cu–Nap, an exothermic event was noticed in the range of 210 to 453 °C, which was responsible for two major mass losses, together totaling 79.32%. This was likely related to the oxidation of two naproxenate molecules (Calcd. 78.95%). The residue of 17.25% was attributed to the formation of copper oxide, CuO (Calcd. 14.74%). Additionally, a small loss of 3.43% slightly over 100 °C was observed, which indicated the loss of one water molecule (Calcd. 3.34%). The presence of one water molecule corroborated the FTIR results.

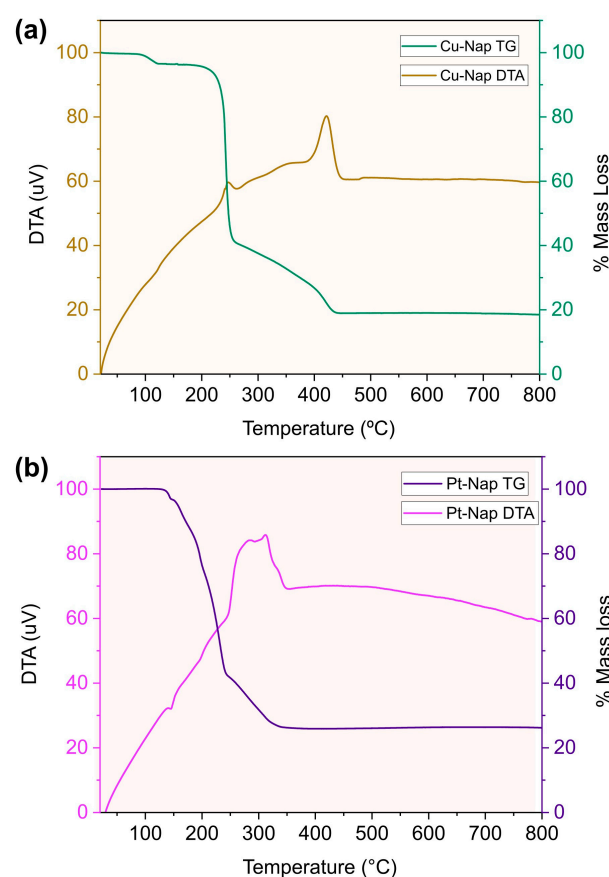


Figure 3. TG/DTA of Cu–Nap and Pt–Nap, from 20 °C to 800 °C, with an increase rate of 10 °C/min of (a) Cu–Nap and (b) Pt–Nap.

For Pt–Nap, TGA indicated a mass loss of 70.61%, from 160 to 350 °C, which likely corresponded to the oxidation of two naproxenate and two DMSO molecules (Calcd. 75.89%). The residue was 26.11%, which matched the composition of PtO (Calcd. 26.08%).

2.4. ESI Mass Spectrometric Analysis

Mass spectrometric analysis of Cu–Nap was conducted to confirm the most probable composition of the complex. The main signals identified in the positive mode (Figure 4a) were at m/z 179.0171 $[(\text{SO}(\text{CH}_3)_2)_2\text{Na}]^+$, seen as $[\text{DMSO}_2 + \text{Na}]^+$, at m/z 448.0435 $[\text{CuC}_{18}\text{H}_{25}\text{O}_5\text{S}_2]^+$ or $[\text{CuNap}(\text{DMSO})_2]^+$, and at m/z 522.0665 $[\text{CuC}_{28}\text{H}_{26}\text{O}_6 + \text{H}^+]$ or $[\text{Cu}(\text{Nap})_2 + \text{H}^+]$ for $z = 1$. Additionally, some important signals were identified in the negative mode (see Figure 4b): 229.0869 $[\text{C}_{14}\text{H}_{13}\text{O}_3]^-$ or Nap^- , 750.1894 $[\text{Cu}(\text{C}_{14}\text{H}_{13}\text{O}_3)_3]^-$

or $[\text{Cu}(\text{Nap})_3]^-$. The signals at m/z 134.8654 and 185.0910 also appeared in the naproxen mass spectrum reported by Zayed et al. [37]. For Pt–Nap (Figure 4c), in the positive mode, the main signals identified were at m/z 231.1011 $[(\text{C}_{14}\text{H}_{14}\text{O}_3) + \text{H}]^+$ or $[(\text{NapH}) + \text{H}]^+$, which is the protonated form of naproxen, and at m/z 253.0830 $[(\text{C}_{14}\text{H}_{13}\text{O}_3\text{Na}) + \text{H}]^+$ or $[(\text{NapNa}) + \text{H}]^+$, corresponding to the protonated form of the NaNap. The $[\text{Pt}(\text{C}_{14}\text{H}_{13}\text{O}_3)_2 + \text{H}]^+$ or $[\text{Pt}(\text{Nap})_2 + \text{H}]^+$ was observed at m/z 653.1401, which corroborated the 1:2 Pt:Nap composition.

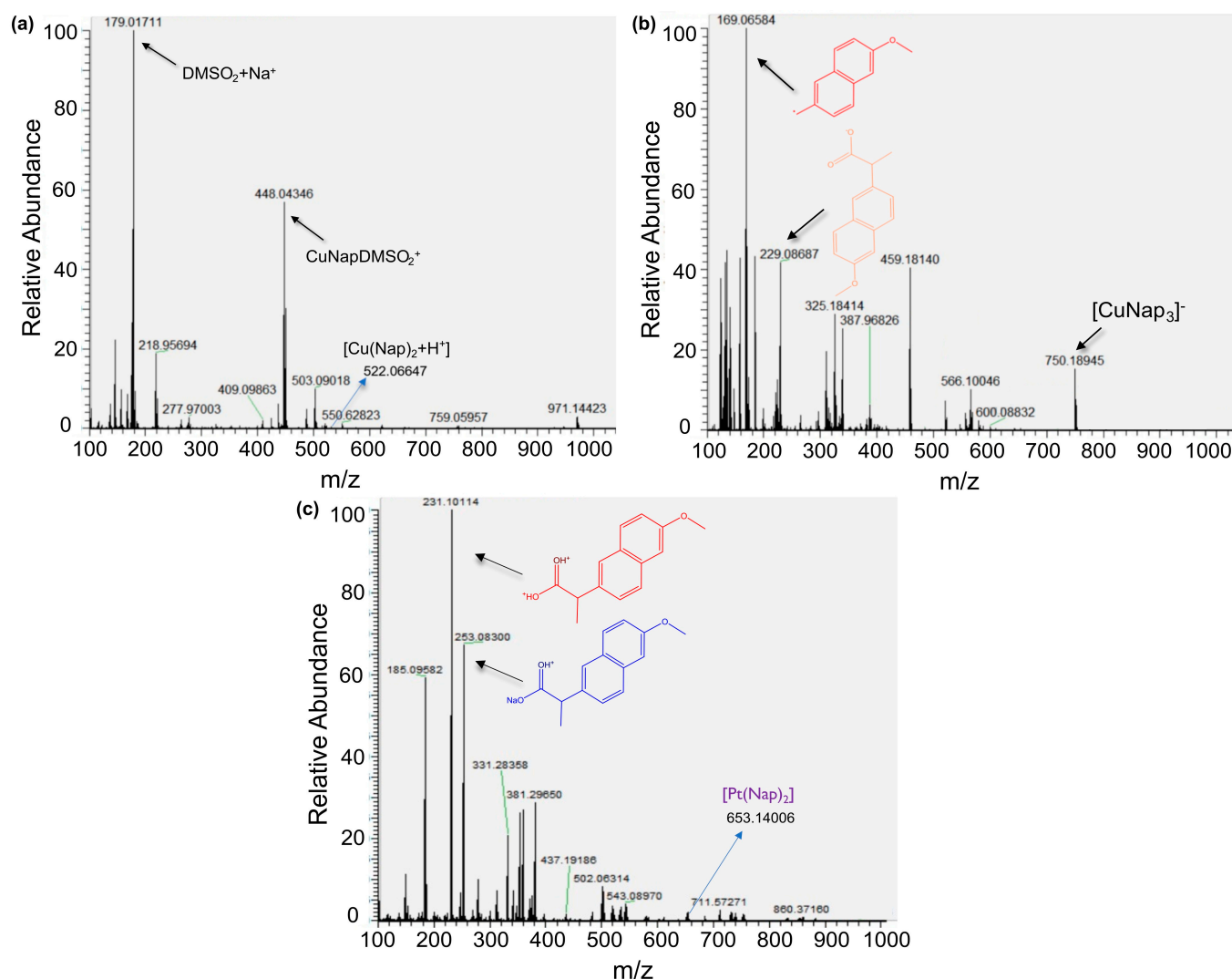


Figure 4. ESI-MS spectra of (a) Cu–Nap in the positive mode, (b) Cu–Nap in the negative mode, and (c) Pt–Nap in the positive mode.

2.5. NMR Measurements

To further evaluate the structure of the Pt–Nap, 1D and 2D NMR spectra were acquired for the complex and sodium naproxenate. The ¹H NMR spectrum of the complex is presented in Figure 5, together with the result for the kinetic study of the solvent exchange (DMSO), with measurements at $t = 0, 12$, and 24 h. The ¹³C NMR spectra of the complex (DMSO-*d*₆) and the ligand (D₂O) are presented in Figures 6a and 6b, respectively. The shifts are numbered according to the attributions for the naproxenate portion corresponding to the schematized molecular structure. The most remarkable information from the ¹H NMR spectrum of the complex was the presence of two signals for DMSO. The signal at 2.50 ppm (quintet, 1H) was attributed to the residual peak of the solvent (CHD₂(SO)CD₃) used in the experiment. The other signal at 2.55 ppm was referred to as DMSO bonded to

platinum (singlet, 6H, $\text{CH}_3(\text{SO})\text{CH}_3$). To facilitate the visualization of both DMSO signals, Supplementary Figure S4 shows the ^1H signals. Moreover, when analyzing the ^{13}C spectra of the complex and the ligand, it was noted that the C1 (carboxylate group) in the complex shifted to a high field with a $\Delta\delta$ of -4.88 . In addition, a small downshift was seen for C2. This observation led us to confirm the coordination of the Nap to Pt(II) by the oxygen atom of the carboxylate group, as will be discussed in the next session.

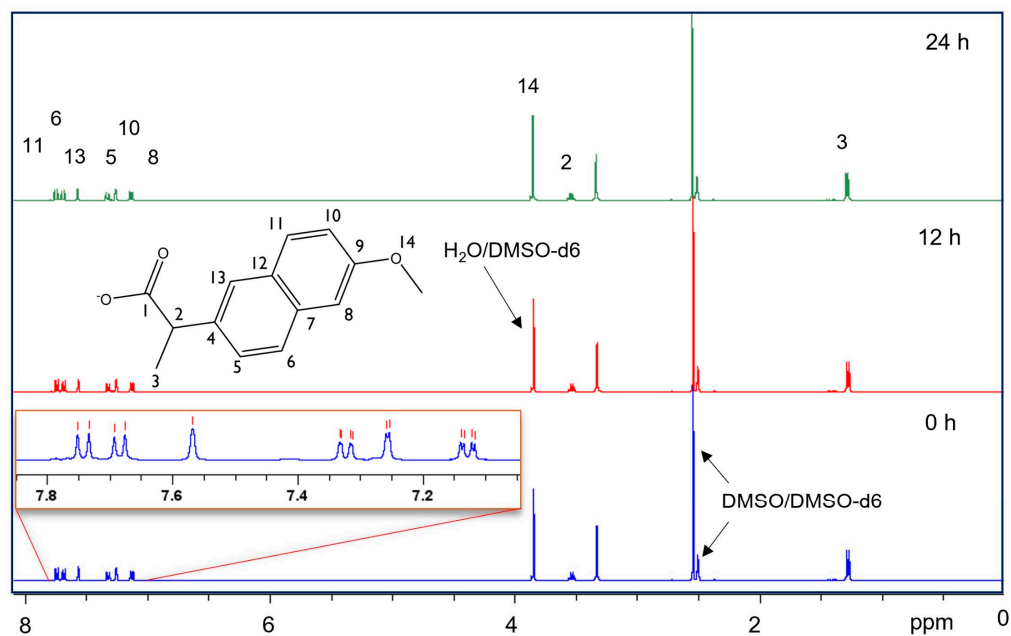


Figure 5. ^1H NMR (500 MHz, DMSO-d_6) spectrum of Pt-Nap in $t = \text{zero h}$, 12 h, and 24 h.

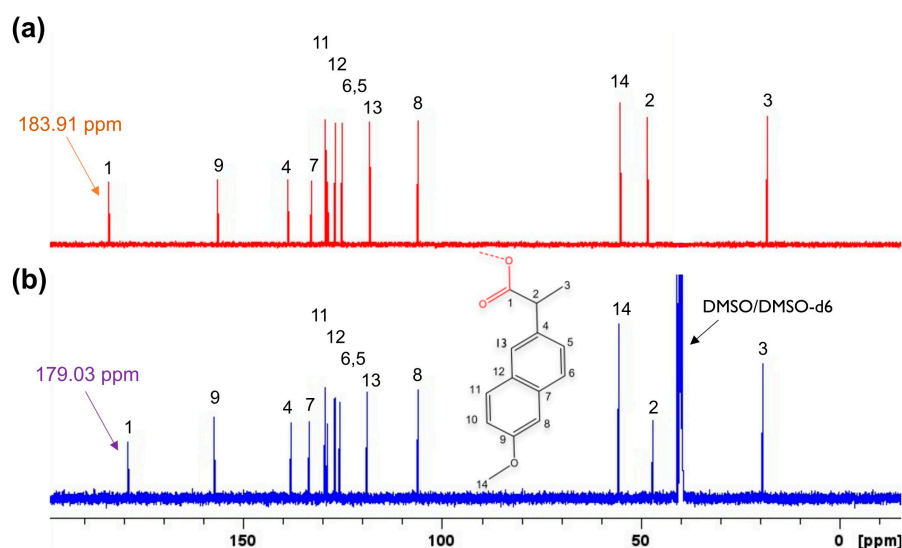


Figure 6. (a) ^{13}C NMR (500 MHz, D_2O) of NaNap; (b) ^{13}C NMR (500 MHz, DMSO-d_6) of Pt-Nap.

Moreover, ^{195}Pt NMR spectroscopic data were also acquired for Pt-Nap (Figure 7) and its starting Pt(II) complex, $\text{cis-}[\text{PtCl}_2(\text{DMSO})_2]$. Potassium hexachloridoplatinate(IV), K_2PtCl_6 was used as a reference, being in accordance with the procedure reported by Quintanilha et al. in the literature [4]. For the precursor, a single peak at -3452.8 ppm was obtained, which was similar to the value of -3445.96 ppm found in the literature [4]. For Pt-Nap, a single peak at -3105.4 ppm was observed, with $\Delta\delta = -347.4$, in comparison to the single peak observed for its precursor.

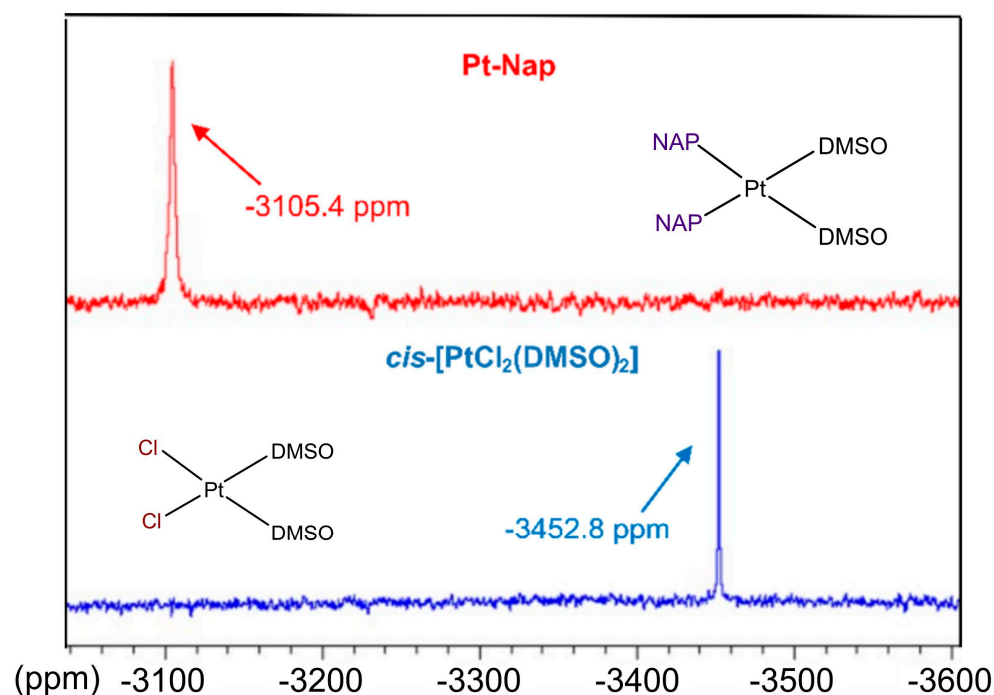


Figure 7. ^{195}Pt NMR spectra for Pt-Nap (top) and $\text{cis-}[\text{PtCl}_2(\text{DMSO})_2]$ (bottom).

2.6. EPR Spectra Analysis

The registered spectra for the complex Cu-Nap (see Figure 8) indicated a paddle-wheel structure, with two copper centers, bridged by four molecules of naproxenate, as observed in the literature [26,27]. The naproxenate molecules were coordinated by the carboxylate groups to both copper centers. At low temperature (77 K), only an isotropic signal was observed, with no hyperfine structure, but at room temperature (293 K), a typical paddle-wheel signal in a binuclear species was detected. Additionally, at room temperature (RT), a radical signal appeared at 350 mT. In the frozen DMSO solution, a central signal probably indicated the formation of a mononuclear species formed by the cleavage of the paddle-wheel structure through the coordination of solvent molecules, with spectroscopic parameters that were quite different from the original binuclear species, as shown in Table 1. The weak signals at ~150 mT and ~470 mT could be attributed to the binuclear species. However, a good fitting with experimental data was not achieved by simulation.

Table 1. EPR parameters determined for the complex Cu-Nap in a solid state and in a frozen DMSO solution.

Temperature	g_x	g_y	g_z	A_x	A_y	A_z
Solid at room temperature	1.9072	2.0430	2.5026	187 G	17 G	200 G
Solid at 77 K		g_{iso} 2.1780			A_{iso} 16 G	
In DMSO solution at 77 K	$g_{\perp} = 2.0355$	$g_{//} = 2.3479$			$A_{//} = 137 \text{ G}$	

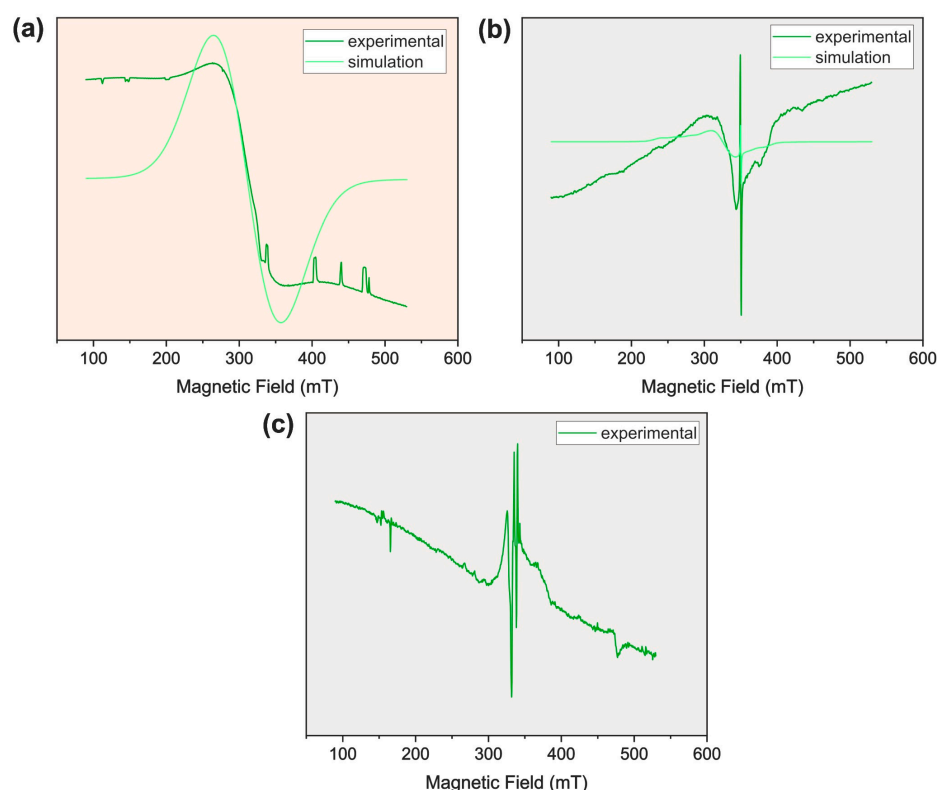


Figure 8. EPR spectra of complex Cu–Nap, registered in a solid state (a) at 77 K and (b) at RT (293 K) and (c) in a DMSO frozen solution at 77 K. In black, experimental results; in red, simulation data.

2.7. Evaluation of Biological Activities

In the disc diffusion assay, the respective masses of each compound added to the discs were calculated, based on the initial concentration of their solutions and molar masses. In these experimental conditions, none of the naproxenate complexes induced growth inhibition of Gram-positive (*S. aureus* and *B. cereus*) or Gram-negative (*E. coli* and *P. aeruginosa*) strains. Considering the starting materials, only copper(II) chloride showed inhibition zones against *S. aureus*, *B. cereus*, and *E. coli* (Table 2).

Table 2. Disc diffusion assay for the naproxenate complexes (Pt–Nap and Cu–Nap) and the starting materials (CuCl₂·2H₂O, NaNap and *cis*-[PtCl₂(DMSO)₂]).

Compounds	MW	Mass	Inhibition Zone (mm)			
			<i>S. aureus</i>	<i>B. cereus</i>	<i>E. coli</i>	<i>P. aeruginosa</i>
CuCl ₂ ·2H ₂ O	170.48	1.549	11.0 (±0.5)	14.0 (±1.0)	11.0 (±0.3)	NI
NaNap	252.24	1.088	NI	NI	NI	NI
<i>cis</i> [PtCl ₂ (DMSO) ₂]	422.25	1.353	NI	NI	NI	NI
Cu–Nap *	1080.12	0.965	NI	NI	NI	NI
Pt–Nap	809.85	1.042	NI	NI	NI	NI

MW = g/mol; Mass = in disc (mg); NI = no inhibition; * (binuclear).

When evaluated against a panel of human tumor cell lines, the copper(II) naproxenate complex Cu–Nap showed a cytostatic effect against glioblastoma (U251, GI₅₀ = 15 µg/mL, SI = 5.7), and multidrug resistant ovarian adenocarcinoma (NCI-ADR/Res, GI₅₀ = 44.3 µg/mL, SI = 1.9) (Figure 9e, Table 3), while platinum naproxenate complex Pt–Nap was inactive (GI₅₀ > 150 µg/mL). Both platinum chloride and sodium naproxenate were inactive (GI₅₀ > 150 µg/mL), while copper(II) chloride showed an unspecific cytostatic activity against all tumor cell lines evaluated (GI₅₀ = 15 µg/mL, TGI = 105.9 µg/mL or 98.0 µmol/L, SI = 2.8) (Figure 9, Table 3).

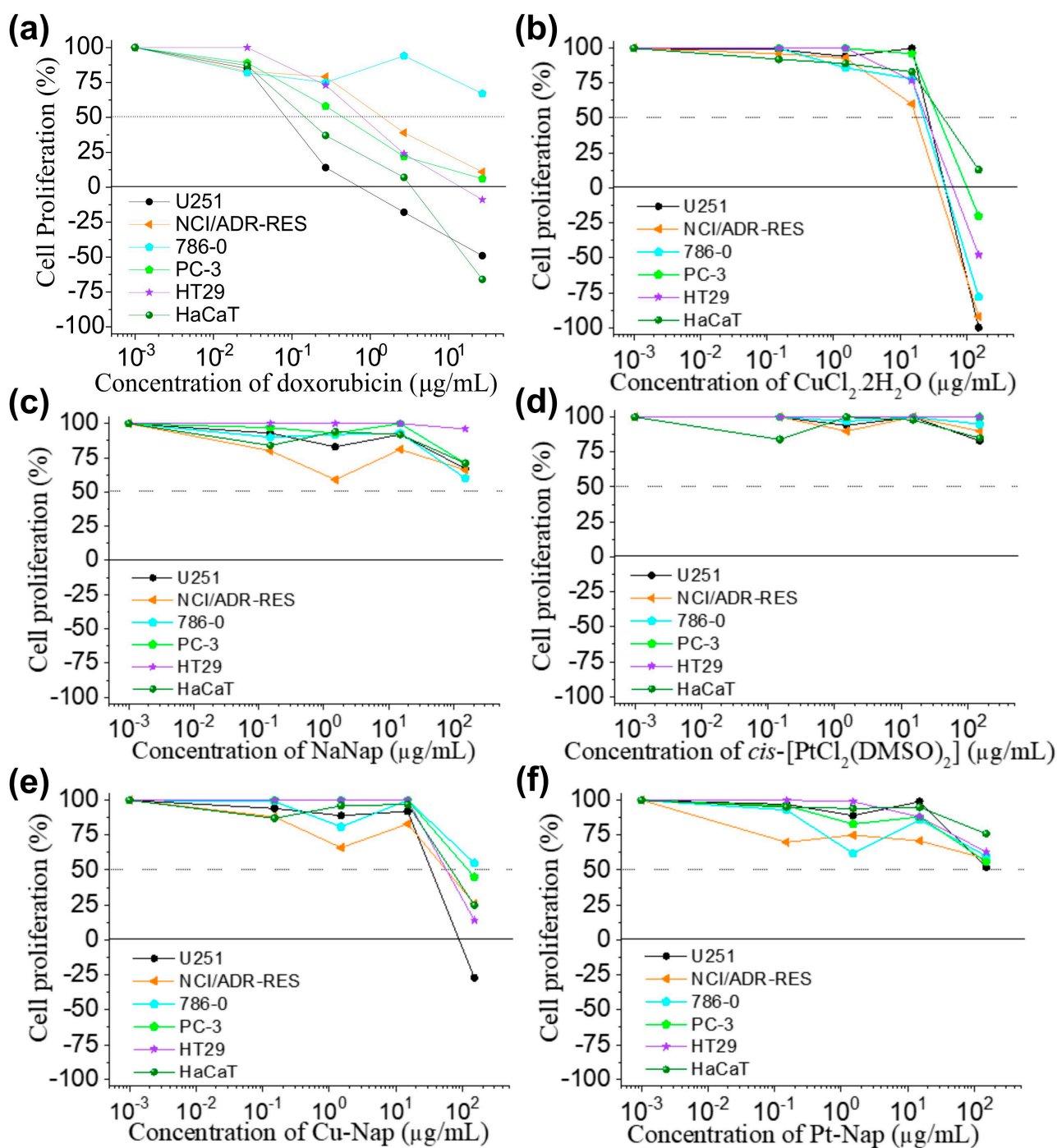


Figure 9. Anti-proliferative profile (%) of (a) doxorubicin (positive control); (b) $\text{CuCl}_2 \cdot 2\text{H}_2\text{O}$; (c) $\text{cis-[PtCl}_2(\text{DMSO})_2]$; (d) NaNap; (e) Cu-Nap; (f) Pt-Nap. Human tumor cell lines: U251 = glioblastoma; NCI-ADR/RES = multidrug resistant ovarian adenocarcinoma; 786-0 = adenocarcinoma of kidney; PC-3 = adenocarcinoma of prostate; HT-29 = adenocarcinoma colorectal. Human non-tumor cell line: HaCaT (immortalized keratinocyte). Sample concentration: 0.15–150 $\mu\text{g/mL}$ (naproxenate complexes and starting material); 0.015–15 $\mu\text{g/mL}$ (doxorubicin). Time exposure = 48 h.

Table 3. Anti-proliferative effect expressed as concentration required to inhibit 50% of growth (GI_{50} , in $\mu\text{g/mL}$) for NaNap, $\text{CuCl}_2 \cdot 2\text{H}_2\text{O}$, Cu–Nap, $\text{cis-PtCl}_2(\text{DMSO})_2$, Pt–Nap, and doxorubicin.

Cell Line	NaNap	$\text{CuCl}_2 \cdot 2\text{H}_2\text{O}$	Cu–Nap	$[\text{PtCl}_2(\text{DMSO})_2]$	Pt–Nap	Doxorubicin
U251	>150	15 *	15 *	>150	>150	0.05 ± 0.03
NCI/ADR-RES	>150	15 *	44.3 ± 62.7	>150	>150	0.8 ± 0.3
786-0	>150	15 *	>150	>150	>150	>15
PC-3	>150	15 *	147.2 ± 0.1	>150	>150	0.25 ± 0.01
HT29	>150	15 *	127.6 ± 0.1	>150	>150	0.4 ± 0.1
HaCaT	>150	42.3 ± 14.2	86.0 ± 37.8	>150	>150	0.092 ± 0.006

Results expressed as concentration required to elicit 50% (GI_{50}) in $\mu\text{g/mL}$ followed by standard error, calculated by sigmoidal regression using Origin 8.0 software; * approximated effective concentration (standard error higher than calculated concentration). Human tumor cell lines: U251 = glioblastoma; NCI-ADR/RES = multidrug resistant ovarian adenocarcinoma; 786-0 = adenocarcinoma of kidney; PC-3 = adenocarcinoma of prostate; HT-29 = adenocarcinoma colorectal. Human non-tumor cell line: HaCaT (immortalized keratinocyte). Sample concentration: 0.15–150 $\mu\text{g/mL}$ (naproxenate complexes and starting material); 0.015–15 $\mu\text{g/mL}$ (doxorubicin). Time exposure = 48 h.

3. Discussion

3.1. Structure, Composition, and Coordination Sphere

Altogether, the results provide insights into the compositions and the coordination sites of naproxenate to the metal ions in the Cu–Nap and Pt–Nap complexes. It is worth mentioning that the formula suggested by elemental analyses and TGA for Cu–Nap was $[\text{Cu}_2(\text{Nap})_4(\text{H}_2\text{O})_2]$, using either $\text{Cu}(\text{NO}_3)_2$ or CuCl_2 as the starting material. This indicates that the anion did not affect the composition of the complex in the synthetic procedure. The proportion of 1 Cu:2 Nap was also identified in the mass spectrum (Figure 4a), with a signal at m/z 522.0665, corresponding to $[\text{Cu}(\text{Nap})_2 + \text{H}]^+$. Moreover, the mass spectrum showed signals with significant abundance in the negative mode and the presence of signals above m/z 520 in the positive mode. Even in low abundance, the signals could be evidence of polymeric or dimeric forms of Cu–Nap. This would explain the poor solubility of the complex in most of the solvents evaluated. The TGA (Figure 3a) indicated that the water molecule was lost at slightly over 100 °C, suggesting that it could be a coordination water rather than a hydration water. This hypothesis was reinforced in the FTIR (Figure 1), with the sharp signal at 3601 cm^{-1} , which was reported in the literature as a coordination water [27]. In addition, when comparing the FTIR spectra of Cu–Nap and NaNap, the $\Delta\nu(\text{COO})$ of 151 cm^{-1} for the complex was a bit lower than that of the ligand, $\Delta\nu(\text{COO}) = 195\text{ cm}^{-1}$. Such data suggests a bidentate bridging coordination mode of carboxylate to copper, just as proposed by Dimiza et al., where a $\Delta\nu$ value was of 170 cm^{-1} for the same complex [27]. This proposition of a paddle-wheel complex differs from the mononuclear copper(II) naproxenate complex $[\text{Cu}(\text{Nap})_2(\text{H}_2\text{O})_3] \cdot \text{H}_2\text{O}$ reported by Chu et al., in which Cu(II) was coordinated by two molecules of nap in the monodentate mode, and three water molecules plus a hydration water [23]. Finally, EPR studies (Figure 8) presented a typical pattern of paddle-wheel structure, confirming our hypothesis.

Furthermore, in the UV spectrum Cu–Nap preserved the naproxenate bands with no significant shifts. The broad low-intensity band that appeared for Cu–Nap at around 700 cm^{-1} corresponded to absorption in red, which matched the greenish color observed in the material. The UV–Vis kinetic study of the Cu–Nap complex in DMSO suggested little ligand exchange of a water molecule by DMSO throughout time (Supplementary Figure S3).

For instance, Pt–Nap presented higher solubility than Cu–Nap in various solvents. Its composition of $\text{PtC}_{32}\text{H}_{38}\text{O}_8\text{S}_2$, or $[\text{Pt}(\text{DMSO})_2(\text{Nap})_2]$ determined by elemental analysis, was confirmed in TGA measurements (Figure 3b), with the loss of two Nap and two DMSO. The proportion of 1 Pt:2 Nap was also confirmed by mass spectrometric data with the presence of the $[\text{Pt}(\text{C}_{14}\text{H}_{13}\text{O}_3)_2 + \text{H}]^+$ ion or $[\text{Pt}(\text{Nap})_2 + \text{H}]^+$ (Figure 4c), at m/z 653.1401. The presence of DMSO in the complex was also reinforced by the FTIR (Figure 1) and Raman (Figure 2) spectroscopic data. Bands attributed to the $\nu(\text{SO})$ at $1144/1129\text{ cm}^{-1}$ and $\nu(\text{PtS})$ at 523 cm^{-1} stretching modes were identified. Due to the presence of a band and a shoulder

for the stretching mode of the sulfoxide group, a cis configuration was proposed [35]. Finally, the presence of coordinated DMSO molecules to Pt(II) was confirmed by ^1H NMR spectroscopic measurements, as shown in Figure 5 and Figure S4.

The final evidence of the coordination sphere of Pt(II) in Pt–Nap comes from the FTIR (Figure 1, Figures S1 and S2) and Raman (Figure 2) stretchings. When analyzing the FTIR spectra of Pt–Nap, the $\Delta(\text{COO})$ of 296 cm^{-1} was higher than that of the ligand ($\Delta 195\text{ cm}^{-1}$). This suggested a monodentate mode of coordination between the carboxylate and Pt(II), according to Dendrinou-Samara et al. [32]. Evidence of Pt(II) bonding to the carboxylate was seen in Raman and far-FTIR, with the presence of $\nu(\text{PtO})$ stretching. The coordination of Pt(II) to the DMSO molecules occurred by the sulfur atom, which was confirmed by the presence of $\nu(\text{PtS})$ stretchings on Raman spectra [35].

Additionally, the ^{13}C NMR spectrum of the Pt–Nap complex exhibited a significant shift of the carbon atom of the carboxylate group in Pt–Nap when analyzing both ligand (183.91 ppm, D_2O) and complex (179.03 ppm, DMSO-d_6) spectra (Figure 6). Thus, the former $\text{cis-[PtCl}_2(\text{DMSO})_2]$ used in the synthesis had the substitution of both its chlorides for naproxenate molecules. This was evidenced in ^{195}Pt NMR (Figure 7), with the shift of -347.4 ppm relative to the signal for $\text{cis-[PtCl}_2(\text{DMSO})_2]$. In other words, there was less shielding effect and narrower electronic density around Pt(II) in Pt–Nap than in its starting complex. Nevertheless, the presence of a single ^{195}Pt peak for Pt–Nap proved that the sample consisted in only one of the geometric isomers.

3.2. Molecular Modeling

As discussed above, Cu–Nap was proposed in a dimeric/polymeric structure, with a bidentate bridging coordination mode of carboxylate to Cu(II). The paddle-wheel structure (Figure 10) was already suggested for Cu(II) complexes combined to NSAIDs, in studies by Trinchero et al. [26] and Mikuriya et al. [38]. The minimum molar composition of $1\text{Cu(II)}:2\text{Nap}:1\text{H}_2\text{O}$ suggested by elemental analysis, TGA, and mass spectrometric data was considered in the construction of this structure. According to the literature, the water molecules should be placed in apical sites of binuclear Cu(II) paddle-wheel structures [39]. Thus, polymerization occurs by the water molecules, with a Cu–Ow interaction, where Ow refers to the oxygen of water molecules. A polymer with compositions $[\text{Cu}_2\text{Nap}_4]_n$ was previously reported by Abuhijleh et al., where the units were linked via Cu–carboxylate interactions from neighboring units [40]. DFT simulations for the dimeric form are presented in Figure 10b and the bond lengths are presented on Table 4. The results show that the distance between the copper atoms (Cu1–Cu2) was 2.870 Å and that the bonding distance between the oxygen atoms of the ligands and the Cu atoms (Cu–O) ranged from 1.872 Å to 2.556 Å . This was in accordance with the values reported in the literature for Cu(II) paddle-wheel complexes [17,34].

Table 4. Bond lengths for Cu–Nap complex formation.

Bond	Distance (Å)	Bond	Distance (Å)
Cu1–O1	2.295	Cu2–O2	1.875
Cu1–O3	2.124	Cu2–O4	1.888
Cu1–O6	2.134	Cu2–O5	1.895
Cu1–O8	2.556	Cu2–O7	1.872
Cu1–Ow1	2.158	Cu2–Ow2	2.343
Cu1–Cu2	2.870		

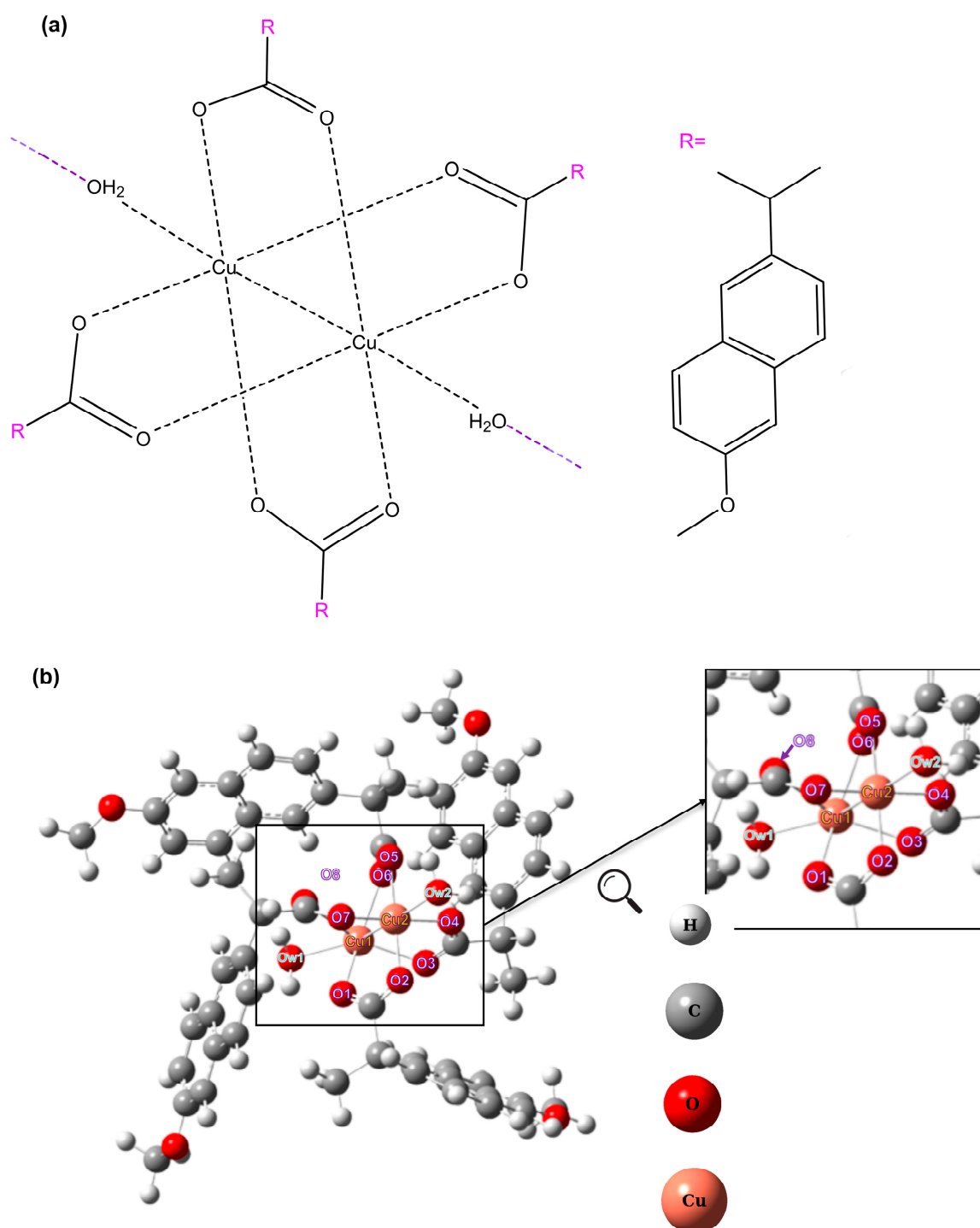


Figure 10. (a) Structural formula for the Cu-Nap complex; (b) molecular model for Cu-Nap.

Furthermore, as previously discussed, it was possible to suggest that Pt-Nap could be seen as $[\text{Pt}(\text{DMSO})_2(\text{Nap})_2]$, with coordination in a monodentate mode of two nap molecules and two DMSO and with the absence of hydration water. Indeed, this coordination mode was also reinforced by the DFT studies. For the Pt-Nap complex, the possibilities of formation of *cis* and *trans* configurations were evaluated, and the structures are presented in Figure 11 with the bond lengths between the central atoms.

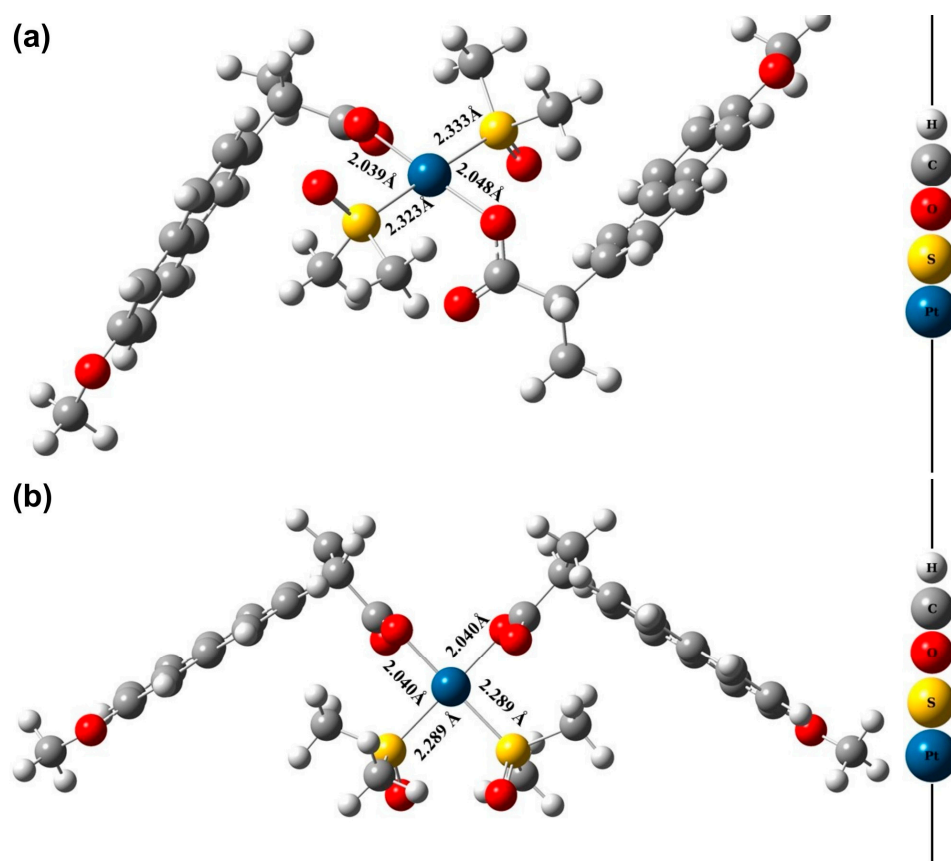


Figure 11. Structural parameters for the complexes: (a) *trans*-[Pt(DMSO)₂(Nap)₂]; (b) *cis*-[Pt(DMSO)₂(Nap)₂].

Analyzing the bond lengths for the *trans*-[Pt(DMSO)₂(Nap)₂] and *cis*-[Pt(DMSO)₂(Nap)₂] configurations, it was possible to observe that the Pt–O and Pt–S bonds length were very close between the structural configurations and the values were in accordance with the distances typically found in complexes in the literature [41].

The electronic energies values were calculated at the M06-2X/6-31 + G(d,p)/LANL2DZ level for the two conformations. It was possible to determine that the energy difference between the complexes *cis* and *trans* was 0.9 kcal mol^{−1}. This allowed us to infer that both isomers may occur. It should be noted that Pereira et al. [42] studied the formation of amantadine (atd), rimantadine (rtd), and memantine (mnt) complexes with platinum [PtCl₂(atd)(DMSO)], [PtCl₂(mnt)(DMSO)], and [PtCl₂(rtd)(DMSO)], and the crystallographic data showed the *cis* configuration for the complex [PtCl₂(mnt)(DMSO)] and *trans* for [PtCl₂(atd)(DMSO)] and [PtCl₂(rtd)(DMSO)]. Together with the X-ray data, the theoretical results showed that both *cis* and *trans* isomers are equally possible to occur, because the energy difference between the complexes was less than ±2.0 kcal·mol^{−1}, which corroborated with the results found in the present work. However, ¹⁹⁵Pt NMR showed a single peak and ¹H and ¹³C NMR spectra did not show the existence of both isomers, suggesting that only one isomer was formed. With insight into Raman (Figure 2) and FTIR (Supplementary Figure S1) spectra, while comparing Pt–Nap to *cis*-[PtCl₂(DMSO)₂], also presented in literature [35,36], the bands corresponded to the *cis* isomer for Pt–Nap.

3.3. Biological Activity Assays

Antibacterial activities were not observed for the Pt–Nap and Cu–Nap complexes or for NaNap and *cis*-[PtCl₂(DMSO)₂] under the considered experimental conditions. As expected [43], CuCl₂·2H₂O showed antibacterial activity against *S. aureus*, *B. cereus*, and *E. coli*. Considering the stability assay results that showed that Cu–Nap appeared to exhibit

only a small ligand exchange in DMSO, especially during the first 8 h (Supplementary Figure S3), the lack of effect can be partially explained by the impaired diffusion rate of Cu–Nap in agar medium [44].

Moreover, the unspecific cytostatic effect observed for copper chloride against tumor cell lines was modulated by the ligand naproxenate, as Cu–Nap selectively inhibited the proliferation of U251 (glioblastoma) and NCI–ADR/Res (multidrug resistant ovarian adenocarcinoma) cell lines (Figure 9). Copper ions have been described as inducing differently regulated cell death mechanisms, such as apoptosis and cuproptosis [45]. Despite the absence of an anti-proliferative effect, naproxen has been regarded as an efficient agent against different *in vivo* cancer models, by modulating the inflammatory microenvironment [46].

Furthermore, the promising cytostatic effects of Cu–Nap against the U251 and NCI–ADR/Res cell lines were accompanied by a weak anti-proliferative effect on the non-tumor cell line (Figure 9). As an on-target toxicological parameter [47], the selectivity index ($SI > 2$) indicated that Cu–Nap may inhibit tumor proliferation in preclinical models, without affecting normal tissues such as mucosa and bone marrow.

It is important to note that Pt–Nap showed stability in DMSO throughout 24 h (Figure 5). Thus, the lack of biological activities observed for Pt–Nap (Figure 9) could not be attributed to instability under experimental conditions. Indeed, no unwanted precipitation or color change was observed during the experimental procedures.

4. Materials and Methods

4.1. Materials and Equipment

Sodium naproxenate (NaNap) (98%), $\text{CuCl}_2 \cdot 2\text{H}_2\text{O}$ (99%), and $\text{cis-[PtCl}_2(\text{DMSO})_2]$ (97%) were purchased from Sigma–Aldrich Laboratories (St. Louis, MO, USA). Dimethylsulfoxide (99.9%) was purchased from Synth (Diadema, Brazil). Elemental analyses were performed on a Perkin Elmer 2400 CHNS/O Analyzer (Shelton, CT, USA). Electronic absorption spectra in the range of 190 to 1100 nm were acquired using a 1.0 cm quartz cuvette in a diode array Hewlett Packard HP8453 UV/Vis absorption spectrophotometer (Shanghai, China). Infrared spectroscopic measurements (FTIR) were performed by using Agilent Cary 630 and 660 FTIR spectrometers (Penang, Malaysia) in the attenuated total reflectance (ATR) method. The FTIR spectra were recorded from 100 to 4000 cm^{-1} , with resolution of 2 cm^{-1} . Raman spectra from 0 to 1500 cm^{-1} were recorded using a Horiba Labram Soleil spectrometer (Loos, France). The thermal stability of the complexes was analyzed using a TGA/DTA simultaneous analyzer SEIKO EXSTAR 6000 (Oyama, Japan). The compounds were evaluated in oxidant atmosphere using an α -alumina crucible, at 25 to $900\text{ }^\circ\text{C}$ with a heating rate of $10\text{ }^\circ\text{C}/\text{min}$. The ^1H , ^{13}C and the $\{^{13}\text{C}, ^1\text{H}\}$ HSQC and HMBC nuclear magnetic resonance (NMR) spectra of NaNap and Pt–Nap were recorded in a Bruker Avance III 500 MHz (11.7 T) spectrometer, while kinetic study of the Pt–Nap was conducted in a Bruker Avance III 400 MHz (9.4 T) NMR spectrometer (Wissembourg, France). Samples were analyzed at 298 K. NaNap was analyzed in D_2O , while the Pt–Nap was dissolved in DMSO-d_6 , due to its solubility in this solvent. The chemical shifts for all solution measurements were provided, relative to tetramethylsilane (TMS). Electrospray ionization mass spectrometry (ESI-MS) measurements were conducted in a Thermo Q-Exactive using a Q-Orbitrap (Bremen, Germany). Samples were evaluated in the positive mode. Cu–Nap was also evaluated in the negative mode. Each solution was directly infused into the instrument's ESI source with capillary potential of 3.50 kV and a source temperature of $300\text{ }^\circ\text{C}$. The dilution used was of $50\times$ with $\text{MeOH:H}_2\text{O}$ 1:1 *v/v*, adding, when necessary, a second injection with 0.1% of formic acid. For Cu–Nap, direct preparation in methanol was not possible due to the low solubility of the material, so a solubilization in DMSO was carried out prior to the dilution in $\text{MeOH:H}_2\text{O}$. The prepared copper complex Cu–Nap was characterized by EPR spectroscopy, registering spectra in a CW–Bruker spectrometer model EMX (Ettlingen, Germany), working at X-band (9.5 GHz, 20.12 mW, 100 kHz modulation frequency) in solid state, and in frozen DMSO solutions. Samples were analyzed at RT (293 K) and at low temperature (77 K) in Wilmad (Vineland, NJ, USA) quartz tubes (4 mm

internal diameter), using a quartz Dewar (Vineland, NJ, USA) with liquid nitrogen for the low temperature measurements. DPPH (α, α' -diphenyl- β -picrylhydrazyl) was used as the frequency calibrant, with $g = 2.0036$. Simulations of spectra were performed with EasySpin software (version 5.2.35) in the MATLAB environment [48].

4.2. Synthesis of Cu(II) Complex with Naproxenate (Cu–Nap)

To synthesize Cu–Nap, $\text{CuCl}_2 \cdot 2\text{H}_2\text{O}$ (0.25×10^{-3} mol) was first dissolved in 5.0 mL of deionized water. This solution was added dropwise to 5.0 mL of an aqueous solution of NaNap (0.50×10^{-3} mol) and maintained under constant stirring for 2 h at room temperature. The solid formed was filtered off under vacuum, washed with distilled water, and dried in a desiccator under P_4O_{10} . Anal. Calcd. for $[\text{Cu}_2(\text{Nap})_4(\text{H}_2\text{O})_2]$ (%): C, 62.27; H, 5.23. Found (%): C, 62.24; H, 5.42. Yield 79.04%. Nap refers to naproxenate. Additionally, the same procedure was performed by using $\text{Cu}(\text{NO}_3)_2 \cdot 3\text{H}_2\text{O}$ as the starting material and the elemental analysis was similar to the first method. Anal. Calcd. for $[\text{Cu}_2(\text{Nap})_4(\text{H}_2\text{O})_2]$ (%): C, 62.27; H, 5.23. Found (%): C, 61.93; H, 5.40. Yield 71.32%. The complex is soluble in DMSO, and poorly soluble in methanol and chloroform. It is insoluble in water.

4.3. Synthesis of Pt(II) Complex with Naproxenate (Pt–Nap)

For the synthesis of Pt–Nap, $\text{cis-}[\text{PtCl}_2(\text{DMSO})_2]$ (0.25×10^{-3} mol) was first dissolved in 5.0 mL of DMSO. This solution was added dropwise to 10 mL of an aqueous solution of NaNap (0.50×10^{-3} mol) and kept under constant stirring for 45 h at room temperature. The solid obtained was collected by filtration under vacuum, washed with distilled water, and dried under P_4O_{10} . Anal. Calcd. for $\text{PtC}_{32}\text{H}_{38}\text{O}_8\text{S}_2$ or $[\text{Pt}(\text{DMSO})_2(\text{Nap})_2]$ (%): C, 46.33; H, 4.86. Found (%): C, 47.46; H, 4.73; Yield 72.61%. Nap refers to naproxenate, while DMSO is dimethylsulfoxide. ^1H NMR (500 MHz, DMSO-d_6) δ (in ppm): 7.74 (d, $J = 8.9$ Hz, 1H), 7.68 (d, $J = 8.5$ Hz, 1H), 7.57 (s, 1H), 7.32 (dd, $J = 8.6$ Hz, 1H), 7.26 (s, 1H), 7.13 (dd, $J = 6.3$ Hz, 1H), 3.85 (s, 3H), 3.54 (q, $J = 7.2$ Hz, 1H), 2.55 (s, 6H), 1.28 (d, $J = 7.2$ Hz, 3H); ^{13}C NMR (500 MHz, DMSO-d_6) δ (in ppm): 179.03, 157.40, 137.94, 133.51, 129.54, 128.87, 127.15, 126.88, 125.80, 118.92, 106.28, 55.58, 47.05, 19.41. Although the percentage of carbon in the elemental analysis was outside the 0.4% range when compared to the expected results, the composition of the complex seemed to be the most reasonable one based on the hydrogen experimental percentage and the thermogravimetric and mass spectrometric data (Sections 2.3 and 2.4).

The complex is soluble in DMSO, dichloromethane, acetone, acetonitrile, and chloroform, and it is poorly soluble in methanol. The complex is insoluble in water.

4.4. Antibacterial Activity Assays In Vitro

Gram-positive *Staphylococcus aureus* (ATCC 25923) and *Bacillus cereus* (ATCC 14579), and Gram-negative *Escherichia coli* (ATCC 25922) and *Pseudomonas aeruginosa* (ATCC 27583) were acquired from the cell culture collection of Fundação André Tosello (Campinas, Brazil). The bacterial strains were inoculated in tubes containing BHI (Brain Heart Infusion FASVI) and incubated for 18 h at 35–37 °C. The disc diffusion method (antibiogram) was applied following the protocol described in the literature [49]. Sterile filter paper discs (Whatman 3 with 10.0 mm in diameter) were impregnated with 50 μL of Pt–Nap, Cu–Nap, and starting material solutions in triplicate. The amount of compound in each disc ranged from 0.96 to 1.55 mg. The impregnated discs were placed on the surface of the solid agar inoculated with a suspension, on the McFarland nephelometric scale 0.5 ($\sim 1.5 \times 10^8$ CFU/mL), of each strain, using a sterile cotton swab. The plates were incubated for 18 h at 35 °C. The sensitivity of the complexes was evaluated from the diameter of the zones of inhibition (in millimeters). $\text{CuCl}_2 \cdot 2\text{H}_2\text{O}$ was used as the positive control.

4.5. Antiproliferative Activity Assay over Tumor and Normal Cells

The anti-proliferative activities of the Pt–Nap and Cu–Nap complexes were evaluated against five human tumor cell lines (U251 = glioblastoma, NCI-ADR/RES = multidrug

resistant ovarian adenocarcinoma, 786-0 = adenocarcinoma of kidney, PC-3 = adenocarcinoma of prostate, and HT-29 = adenocarcinoma colorectal) and one human non-tumor cell line (HaCaT, immortalized keratinocyte). The tumor cell lines were kindly provided by the Frederick Cancer Research & Development Center, National Cancer Institute, Frederick, MA, USA, while the non-tumor cell line was provided by Dr. Ricardo Della Coletta (UNICAMP).

Stock cultures were grown in RPMI-1640 (Vitrocell, Brazil) supplemented with 5% fetal bovine serum (Vitrocell, Brazil) (complete medium) at 37 °C in 5% CO₂. For the experiments, complete medium was supplemented with a 1% penicillin:streptomycin mixture (Nutricell, Brazil, 1000 U/mL:1000 mg/mL). Aliquots of CuCl₂, *cis*-PtCl₂, Pt-Nap, Cu-Nap, and NaNap were dissolved in DMSO (1.0 mg material: 10 µL DMSO). Afterwards, each sample solution (50 µL) was diluted in the complete medium (5000 µg/mL), followed by a serial dilution affording the final concentrations of 0.15, 1.5, 15, and 150 µg/mL. Doxorubicin (0.015, 0.15, 1.5, and 15 µg/mL) was used as the positive control. The DMSO final concentration (≤0.15%) did not affect cell viability [50].

Cells in 96-well plates (100 µL cells/well, inoculation density: 3.5 to 6 × 10⁴ cell/mL) were exposed to four concentrations of each sample and doxorubicin (100 µL/well), in triplicate, for 48 h at 37 °C and 5% of CO₂. Before (T₀ plate) and after (T₁ plates) the sample addition, the cells were fixed with 50% trichloroacetic acid (50 µL/well), and the cell proliferation was determined by the spectrophotometric quantification of cellular protein content using the sulforhodamine B assay [51]. The measurements were taken at 540 nm in a VersaMax Molecular Devices spectrometer (San Jose, CA, USA). The sample concentration that inhibits 50% cell growth (GI₅₀, cytostatic effect) was calculated via sigmoidal regression using Origin 9.0 software (OriginLab Corporation, Northampton, MA, USA) [52]. The selectivity index [47] was calculated as described in Equation (1).

$$SI = (GI_{50 \text{ HaCaT}} / GI_{50 \text{ TCL}}), \text{ where TCL = tumor cell line} \quad (1)$$

4.6. Computational Simulations

Gaussian 09 [53] and GaussView [54] programs were used for the computational simulation and to generate the structures of the compounds, respectively. Density functional theory (DFT) was used to evaluate the complexation of platinum and copper metal atoms with the sodium naproxenate ligand, Cu-Nap, and Pt-Nap complexes. For the simulations, the functional M06-2X [55] with 6-31 + G(d,p) [56–58] basis set for hydrogen, carbon, oxygen, and sulfur atoms and the LANL2DZ [59] effective core basis set for copper and platinum atoms were used. Frequency calculations were performed, and no imaginary frequency was found, which confirmed that the optimized structures were at minimum energy.

5. Conclusions

Our study described an efficient strategy to synthesize platinum(II) and copper(II) complexes, with naproxenate as the ligand. The complexes were successfully synthesized and characterized by chemical, spectroscopic, and molecular modeling analyses. Antiproliferative studies were conducted for bacteria and tumor cells, for evaluation of the biological activities of each complex.

Molecular formulae of the complexes were determined, by elemental and thermal analyses, as [Cu₂(Nap)₄(H₂O)₂] for Cu-Nap and [Pt(DMSO)₂(Nap)₂] for Pt-Nap. The coordination of Nap to Cu(II) occurred by the oxygen atoms of the carboxylate group in a bridging bidentate fashion. Mass spectrometric data, EPR, and molecular modeling optimization suggested the formation of a binuclear species for the Cu-Nap complex in a dimeric, or even polymeric, form, which explains its low solubility in most solvents. EPR spectra reinforced the existence of a binuclear species. In the DMSO solution, formation of mononuclear species occurred via the cleavage of the binuclear complex.

Conversely, infrared and NMR spectroscopic data permitted a proposal of a monodentate coordination of two Nap molecules to Pt(II). The square-planar coordination sphere

was completed by two DMSO molecules, as indicated by elemental, infrared, and NMR spectroscopic analyses.

Preliminary antibacterial activity assays showed that the bacterial strains considered in the experiment were resistant to both complexes at the concentrations tested. However, while Pt–Nap did not present inhibition over 50% of the tumor cell lines' growth, Cu–Nap presented a significant cytostatic effect against HT-29 and PC-3 and a low but significant cytotoxic effect over the U251 tumor cell line. The cell viability of the complexes was assessed against the HaCaT cell line, and Pt–Nap presented extremely low cytostatic effect at all concentrations assessed, as did its precursor NaNap. However, Cu–Nap presented a cytostatic effect of over 50%, with a GI_{50} of 86 $\mu\text{g/mL}$ (79.6 $\mu\text{mol/L}$). Still, it showed some selectivity over U251 tumor cells. Altogether, while the Pt(II) complex seems to be poorly effective, the obtained data concerning the biological activity of the Cu(II) complex with naproxen open new perspectives about its use as a cytotoxic agent over tumor cells. Further in vitro and in vivo studies are needed to confirm this hypothesis.

Supplementary Materials: The following supporting information can be downloaded at: <https://www.mdpi.com/article/10.3390/inorganics11080331/s1>, Figure S1: ATR–FTIR of Pt–Nap and NaNap from 1300 to 500 cm^{-1} . Figure S2: ATR–FTIR of Pt–Nap and NaNap from 1300 to 500 cm^{-1} . Figure S3: Kinetic UV–Vis of Cu–Nap in 24h at absorbances peaks 260, 275, 320, and 335 nm. Figure S4: ^1H NMR with integrals. Inset shows both DMSO signals, coordinated in Pt–Nap and solvent.

Author Contributions: A.A.S.: writing—original draft preparation, review and editing, conceptualization, visualization, methodology, investigation, formal analysis, and validation; S.C.L.F.: investigation; Á.B.C.: investigation; K.E.B.: investigation; D.D.A.: investigation; M.C.P.: investigation; A.L.T.G.R.: conceptualization, investigation, writing—review and editing, project administration, supervision, and funding acquisition; J.E.d.C.: investigation, project administration, supervision, and funding acquisition; W.R.L.: conceptualization, investigation, and funding acquisition; D.H.P.: methodology, investigation, funding acquisition, and writing—original draft preparation; A.M.d.C.F.: writing—original draft preparation, review and editing, methodology, and investigation; P.P.C.: conceptualization, visualization, investigation, writing—review and editing, formal analysis, project administration, supervision, and funding acquisition. All authors have read and agreed to the published version of the manuscript.

Funding: The authors thank CAPES (Financial code 001), FAPESP (2018/12062-4; 2021/07458-9, 2021/08717-8 and 2021/10265-8 Cancer Theranostics Innovation Center CancerThera, CEPID), FAEPEX (2432/22), and CNPq (407012/2018-4) for the financial support. Marcelo C. Portes and A.M. da Costa Ferreira thank CEPID-Redoxoma (FAPESP grant 2013/07937-8) for maintenance of EPR equipment. A.L.T.G. Ruiz thanks the National Council for Scientific and Technological Development (CNPq, grants #429463/2018-9 and #313440/2019-0), the São Paulo Research Foundation (FAPESP #2011/01114-4, #2014/23950-7), and the Fund for Support to Teaching, Research and Outreach Activities of the University of Campinas (FAEPEX/Unicamp, grants #2001/19, #2555/20, and #2235/21).

Data Availability Statement: Not applicable.

Conflicts of Interest: The authors declare no conflict of interest.

References

1. Gomes, F.R.; Addis, Y.; Tekamo, I.; Cavaco, I.; Campos, D.L.; Pavan, F.R.; Gomes, C.S.B.; Brito, V.; Santos, A.O.; Domingues, F.; et al. Antimicrobial and antitumor activity of *S*-methyl dithiocarbazate Schiff base zinc(II) complexes. *J. Inorg. Biochem.* **2021**, *216*, 111331. [\[CrossRef\]](#)
2. Manzano, C.M.; Bergamini, F.R.G.; Lustri, W.R.; Ruiz, A.L.T.G.; De Oliveira, E.C.S.; Ribeiro, M.A.; Formiga, A.L.B.; Corbi, P.P. Pt(II) and Pd(II) complexes with ibuprofen hydrazide: Characterization, theoretical calculations, antibacterial and antitumor assays and studies of interaction with CT-DNA. *J. Mol. Struct.* **2018**, *1154*, 469–479. [\[CrossRef\]](#)
3. Štarha, P.; Trávníček, Z. Non-platinum complexes containing releasable biologically active ligands. *Coord. Chem. Rev.* **2019**, *395*, 130–145. [\[CrossRef\]](#)

4. Quintanilha, M.M.; Schimidt, B.A.; Costa, A.M.F.; Nakahata, D.H.; Simoni, D.A.; Clavijo, J.C.T.; Pereira, D.H.; Massabni, A.C.; Lustri, W.R.; Corbi, P.P. A novel water-soluble platinum(II) complex with the amino acid deoxyallin: Synthesis, crystal structure, theoretical studies and investigations about its antibacterial activity. *J. Mol. Struct.* **2021**, *1236*, 130316. [\[CrossRef\]](#)
5. Silconi, Z.B.; Benazic, S.; Milovanovic, J.; Jurisevic, M.; Djordjevic, D.; Nikolic, M.; Mijajlovic, M.; Ratkovic, Z.; Radić, G.; Radisavljevic, S.; et al. DNA binding and antitumor activities of platinum(IV) and zinc(II) complexes with some S-alkyl derivatives of thiosalicylic acid. *Transit. Metal Chem.* **2018**, *43*, 719–729. [\[CrossRef\]](#)
6. Ravera, M.; Zanellato, I.; Gabano, E.; Perin, E.; Rangone, B.; Coppola, M.; Osella, D. Antiproliferative activity of Pt(IV) conjugates containing the non-steroidal anti-inflammatory drugs (NSAIDs) ketoprofen and naproxen. *Int. J. Mol. Sci.* **2019**, *20*, 3074. [\[CrossRef\]](#)
7. Quirante, J.; Ruiz, D.; Gonzalez, A.; López, C.; Cascante, M.; Cortés, R.; Messegue, R.; Calvis, C.; Baldomà, L.; Pascual, A.; et al. Platinum(II) and palladium(II) complexes with (N,N') and (C,N,N')—Ligands derived from pyrazole as anticancer and antimalarial agents: Synthesis, characterization and in vitro activities. *J. Inorg. Biochem.* **2011**, *105*, 1720–1728. [\[CrossRef\]](#) [\[PubMed\]](#)
8. Fox, C.L. Silver sulfadiazine—A new topical therapy for Pseudomonas in burns. Therapy of Pseudomonas infection in burns. *Arch. Surg.* **1968**, *96*, 184–188. [\[CrossRef\]](#) [\[PubMed\]](#)
9. Leung, C.H.; Lin, S.; Zhong, H.; Ma, D. Metal complexes as potential modulators of inflammatory and autoimmune responses. *Chem. Sci.* **2015**, *6*, 871. [\[CrossRef\]](#) [\[PubMed\]](#)
10. Xun-Zhong, Z.; An-Sheng, F.; Fu-Ran, Z.; Min-Cheng, L.; Yan-Zhi, L.; Meng, M.; Yu, L. Synthesis, Crystal Structures, and Antimicrobial and Antitumor Studies of Two Zinc(II) Complexes with Pyridine Thiazole Derivatives. *Bioinorg. Chem. Appl.* **2020**, *2020*, 8852470. [\[CrossRef\]](#)
11. Frei, A.; Zuegg, J.; Elliott, A.G.; Baker, M.; Braese, S.; Brown, C.; Chen, F.; Dowson, C.G.; Dujardin, G.; Jung, N.; et al. Metal complexes as a promising source for new Antibiotics. *Chem. Sci.* **2020**, *11*, 2627–2639. [\[CrossRef\]](#)
12. Ali, H.A.; Fares, H.; Darawsheh, M.; Rappocciolo, E.; Akkawi, M.; Jaber, S. Synthesis, characterization and biological activity of new mixed ligand complexes of Zn(II) naproxen with nitrogen-based ligands. *Eur. J. Med. Chem.* **2015**, *89*, 67–76. [\[CrossRef\]](#) [\[PubMed\]](#)
13. Oliveira, L.P.; Carneiro, Z.A.; Ribeiro, C.M.; Lima, M.F.; Paixão, D.A.; Pivatto, M.; Souza, M.V.N.; Teixeira, L.R.; Lopes, C.D.; Albuquerque, S.; et al. Three new platinum complexes containing fluoroquinolones and DMSO: Cytotoxicity and evaluation against drug-resistant tuberculosis. *J. Inorg. Biochem.* **2018**, *183*, 77–83. [\[CrossRef\]](#) [\[PubMed\]](#)
14. Juin, S.; Muhammad, N.; Sun, Y.; Tan, Y.; Yuan, H.; Song, D.; Guo, Z.; Wang, X. Multispecific Platinum(IV) Complex Deters Breast Cancer via Interposing Inflammation and Immunosuppression as an Inhibitor of COX-2 and PD-L1. *Angew. Chem. Int.* **2020**, *59*, 23313–23321. [\[CrossRef\]](#)
15. Chen, Y.; Wang, Q.; Li, Z.; Liu, Z.; Zhao, Y.; Zhang, J.; Liu, M.; Wang, Z.; Li, D.; Han, J. Naproxen platinum(IV) hybrids inhibiting cyclooxygenases and matrix metalloproteinases and causing DNA damage: Synthesis and biological evaluation as antitumor agents in vitro and in vivo. *Dalton Trans.* **2020**, *49*, 5192–5204. [\[CrossRef\]](#) [\[PubMed\]](#)
16. Bhattacharjee, P.; Roy, M.; Naskar, A.; Tsai, H.; Ghosh, A.; Patra, N.; John, R.P. A trinuclear copper (II) complex of naproxen-appended salicylhydrazide: Synthesis, crystal structure, DNA binding and molecular docking study. *Appl. Organomet. Chem.* **2022**, *36*, 6459. [\[CrossRef\]](#)
17. Abuhijleh, A.L. Mononuclear and Binuclear Copper (II) Complexes of the Antinflammatory Drug Ibuprofen: Synthesis, Characterization, and Catecholase-Mimetic Activity. *J. Inorg. Biochem.* **1994**, *55*, 255–262. [\[CrossRef\]](#) [\[PubMed\]](#)
18. Nunes, J.H.B.; Paiva, R.E.F.; Cuin, A.; Ferreira, A.M.C.; Lustri, W.R.; Corbi, P.P. Synthesis, spectroscopic characterization, crystallographic studies and antibacterial assays of new copper(II) complexes with sulfathiazole and nimesulide. *J. Mol. Struct.* **2016**, *1112*, 14–20. [\[CrossRef\]](#)
19. Spector, D.; Krasnovskaya, O.; Pavlov, K.; Erofeev, A.; Gorelkin, P.; Beloglazkina, E.; Majouga, A. Pt(IV) Prodrugs with NSAIDs as Axial Ligands. *Int. J. Mol. Sci.* **2021**, *22*, 3817. [\[CrossRef\]](#) [\[PubMed\]](#)
20. Tolan, D.A.; Abdel-Monem, Y.K.; El-Nagar, M.A. Anti-tumor platinum (IV) complexes bearing the anti-inflammatory drug naproxen in the axial position. *Appl. Organometal. Chem.* **2019**, *33*, 4763. [\[CrossRef\]](#)
21. Dimiza, F.; Papadopoulos, A.N.; Tangoulis, V.; Psycharis, V.; Raptopoulou, C.P.; Kessissoglou, D.P.; Psomas, G. Biological evaluation of cobalt(II) complexes with non-steroidal anti-inflammatory drug naproxen. *J. Inorg. Biochem.* **2012**, *107*, 54–64. [\[CrossRef\]](#)
22. Shaheen, M.A.; Feng, S.; Anthony, M.; Tahir, M.N.; Hassan, M.; Seo, S.; Ahmad, S.; Iqbal, M.; Saleem, M.; Lu, C. Metal-Based Scaffolds of Schiff Bases Derived from Naproxen: Synthesis, Antibacterial Activities, and Molecular Docking Studies. *Molecules* **2019**, *24*, 1237. [\[CrossRef\]](#)
23. Chu, Y.; Wang, T.; Ge, X.; Yang, P.; Li, W.; Zhao, J.; Zhu, H. Synthesis, characterization and biological evaluation of naproxen Cu(II) complexes. *J. Mol. Struct.* **2019**, *1178*, 564–569. [\[CrossRef\]](#)
24. Wang, T.; Tang, G.; Wan, W.; Wu, Y.; Tian, T.; Wang, J.; He, C.; Long, X.; Wang, J.; Ng, S.W. New homochiral ferroelectric supramolecular networks of complexes constructed by chiral S-naproxen ligand. *CrystEngComm* **2012**, *14*, 3802. [\[CrossRef\]](#)
25. Hasan, M.S.; Das, N. A detailed in vitro study of naproxen metal complexes in quest of new therapeutic possibilities. *Alex. J. Med.* **2017**, *53*, 157–165. [\[CrossRef\]](#)
26. Trincherio, A.; Bonora, S.; Tinti, A.; Fini, G. Spectroscopic Behavior of Copper Complexes of Nonsteroidal Anti-Inflammatory Drugs. *Biopolymers* **2004**, *74*, 120–124. [\[CrossRef\]](#)

27. Dimiza, F.; Perdihi, F.; Tangoulis, V.; Turel, I.; Kessissoglou, D.P.; Psomas, G. Interaction of copper(II) with the non-steroidal anti-inflammatory drugs naproxen and diclofenac: Synthesis, structure, DNA- and albumin-binding. *J. Inorg. Biochem.* **2011**, *105*, 476–489. [\[CrossRef\]](#) [\[PubMed\]](#)
28. Martins, D.J.; Hanif-Ur-Rehman; Rico, S.A.; Costa, I.M.; Santos, A.C.P.; Szzudlowski, R.G.; Silva, D.O. Interaction of chitosan beads with a copper-naproxen metallodrug. *RSC Adv.* **2015**, *5*, 90184. [\[CrossRef\]](#)
29. Abuhijleh, A.L. Mononuclear copper (II) salicylate complexes with 1,2-dimethylimidazole and 2-methylimidazole: Synthesis, spectroscopic and crystal structure characterization and their superoxide scavenging activities. *J. Mol. Struct.* **2010**, *980*, 201–207. [\[CrossRef\]](#)
30. Sharma, J.; Singla, A.K.; Dhawan, S. Zinc-naproxen complex: Synthesis, physicochemical and biological evaluation. *Int. J. Pharm.* **2003**, *260*, 217–227. [\[CrossRef\]](#)
31. Srivastava, P.; Mishra, R.; Verma, M.; Sivakumar, S.; Patra, A.K. Cytotoxic ruthenium(II) polypyridyl complexes with naproxen as NSAID: Synthesis, biological interactions and antioxidant activity. *Polyhedron* **2019**, *172*, 132–140. [\[CrossRef\]](#)
32. Dendrinou-Samara, C.; Tsotsou, G.; Ekateriniadou, L.V.; Kortsaris, A.H.; Raptopoulou, C.P.; Terzis, A.; Kyriakidis, D.A.; Kessissoglou, D.P. Anti-inflammatory drugs interacting with Zn(II), Cd(II) and Pt(II) metal ions. *J. Inorg. Biochem.* **1998**, *71*, 171–179. [\[CrossRef\]](#)
33. Srivastava, P.; Singh, K.; Verma, M.; Sivakumar, S.; Patra, A.K. Photoactive platinum(II) complexes of nonsteroidal anti-inflammatory drug naproxen: Interaction with biological targets, antioxidant activity and cytotoxicity. *Eur. J. Med. Chem.* **2018**, *144*, 243–254. [\[CrossRef\]](#)
34. Terracina, A.; McHugh, L.N.; Todaro, M.; Agnello, S.; Wheatley, P.S.; Gelardi, F.M.; Morris, R.E.; Buscarino, G. Multitechnique Analysis of the Hydration in Three Different Copper Paddle-Wheel Metal-Organic Frameworks. *J. Phys. Chem. C* **2019**, *123*, 28219–28232. [\[CrossRef\]](#)
35. Price, J.H.; Williamson, A.N.; Schramm, R.F.; Wayland, B.B. Palladium(II) and platinum(II) alkyl sulfoxides complexes. Examples of sulfur-bonded, mixed sulfur- and oxygen-bonded, and totally oxygen-bonded complexes. *Inorg. Chem.* **1972**, *11*, 1280–1284. [\[CrossRef\]](#)
36. Zhang, J.; Li, Y.; Sun, J. Synthesis, characterization and cytotoxicity of amine/ethylamine platinum(II) complexes with carboxylates. *Eur. J. Med. Chem.* **2009**, *44*, 2758–2762. [\[CrossRef\]](#) [\[PubMed\]](#)
37. Zayed, M.A.; Hawash, M.F.; El-Desawy, M.; El-Gizouli, A.M.M. Investigation of naproxen drug using mass spectrometry, thermal analyses and semi-empirical molecular orbital calculation. *Arab. J. Chem.* **2017**, *10*, 351–359. [\[CrossRef\]](#)
38. Mikuriya, M.; Chihiro, Y.; Tanabe, K.; Nukita, R.; Amabe, Y.; Yoshioka, D.; Mitsunashi, R.; Tatehata, R.; Tanaka, H.; Handa, M.; et al. Copper(II) Carboxylates with 2,3,4-Trimethoxybenzoate and 2,4,6-Trimethoxybenzoate: Dinuclear Cu(II) Cluster and μ -Aqua-Bridged Cu(II) Chain Molecule. *Magnetochemistry* **2021**, *7*, 35. [\[CrossRef\]](#)
39. Wang, Z.; Rodewald, K.; Medishetty, R.; Rieger, B.; Fischer, R.A. Control of Water Content for Enhancing the Quality of Copper Paddle-Wheel-Based Metal-Organic Framework Thin Films Grown by Layer-by-Layer Liquid-Phase Epitaxy. *Cryst. Growth Des.* **2018**, *18*, 7451–7459. [\[CrossRef\]](#)
40. Abuhijleh, A.L.; Khalaf, J. Copper (II) complexes of the anti-inflammatory drug naproxen and 3-pyridylmethanol as auxiliary ligand. Characterization, superoxide dismutase and catecholase-mimetic activities. *Eur. J. Med. Chem.* **2010**, *45*, 3811–3817. [\[CrossRef\]](#) [\[PubMed\]](#)
41. Vaz, R.H.; Silva, R.M.; Reibenspies, J.H.; Serra, O.A. Synthesis and X-ray Crystal Structure of a Stable *cis*-1,2-bis(diphenylphosphino)ethene Monodentate Thiolate Platinum Complex and TGA Studies of its Precursors. *J. Braz. Chem. Soc.* **2002**, *13*, 82–87. [\[CrossRef\]](#)
42. Pereira, A.K.S.; Manzano, C.M.; Nakahata, D.H.; Clavijo, J.C.T.; Pereira, D.H.; Lustri, W.R.; Corbi, P.P. Synthesis, crystal structures, DFT studies, antibacterial assays and interaction assessments with biomolecules of new platinum(II) complexes with adamantane derivatives. *New J. Chem.* **2020**, *44*, 11546–11556. [\[CrossRef\]](#)
43. Vincent, M.; Duval, R.E.; Hartemann, P.; Engels-Deutsch, M. Contact killing and antimicrobial properties of copper. *J. Appl. Microbiol.* **2018**, *124*, 1032–1046. [\[CrossRef\]](#)
44. Jorgensen, J.H.; Ferraro, M.J. Antimicrobial susceptibility testing: A review of general principles and contemporary practices. *Clin. Infect. Dis. Off. Publ. Infect. Dis. Soc. Am.* **2009**, *49*, 1749–1755. [\[CrossRef\]](#)
45. Xue, Q.; Kang, R.; Klionsky, D.J.; Tang, D.; Liu, J.; Chen, X. Copper metabolism in cell death and autophagy. *Autophagy* **2023**, *19*, 2175–2195. [\[CrossRef\]](#) [\[PubMed\]](#)
46. Han, M.İ.; Küçükgül, Ş.G. Anticancer and Antimicrobial Activities of Naproxen and Naproxen Derivatives. *Mini Rev. Med. Chem.* **2020**, *20*, 1300–1310. [\[CrossRef\]](#)
47. Muller, P.Y.; Milton, M.N. The determination and interpretation of the therapeutic index in drug development. *Nat. Rev. Drug Discov.* **2012**, *11*, 751–761. [\[CrossRef\]](#)
48. Stoll, S.; Schweiger, A. EasySpin, a comprehensive software package for spectral simulation and analysis in EPR. *J. Magn. Res.* **2006**, *178*, 42–55. [\[CrossRef\]](#)
49. CLSI. *Performance Standards for Antimicrobial Susceptibility Testing*, 32nd ed.; CLSI supplement M100; Clinical and Laboratory Standards Institute: Wayne, PA, USA, 2022.
50. Sobreiro, M.A.; Della Torre, A.; de Araújo, M.E.M.B.; Canella, P.R.B.C.; de Carvalho, J.E.; Carvalho, P.O.; Ruiz, A.L.T.G. Enzymatic hydrolysis of rutin: Evaluation of kinetic parameters and anti-proliferative, mutagenic and anti-mutagenic effects. *Life* **2023**, *13*, 549. [\[CrossRef\]](#)

51. Da Silva, G.G.; Della Torre, A.; Braga, L.E.O.; Bachiega, P.; Tinti, S.V.; de Carvalho, J.E.; Dionísio, A.P.; Ruiz, A.L.T.G. Yellow-colored extract from cashew byproduct—Nonclinical safety assessment. *Regul. Toxicol. Pharmacol.* **2020**, *115*, 104699. [[CrossRef](#)]
52. Monks, A.; Scudiero, D.; Skehan, P.; Shoemaker, R.; Paull, K.; Vistica, D.; Hose, C.; Langley, J.; Cronise, P.; Vaigro-Wolff, A.; et al. Feasibility of a high-flux anticancer drug screen using a diverse panel of cultured human tumor cell lines. *JNCI J. Natl. Cancer Inst.* **1991**, *83*, 757–766. [[CrossRef](#)]
53. Frisch, J.; Trucks, G.W.; Schlegel, H.B.; Scuseria, G.E.; Robb, M.A.; Cheeseman, J.R.; Scalmani, G.; Barone, V.; Mennucci, B.; Petersson, G.A.; et al. *Gaussian09, Revision D.1*; Gaussian, Inc.: Wallingford, CT, USA, 2009.
54. Dennington, R.; Keith, T.; Millam, J. *Gauss View, Version 5*; Shawnee Mission. (n.d.); Semichem Inc.: Shawnee, KS, USA, 2009.
55. Zhao, Y.; Truhlar, D.G. The M06 suite of density functionals for main group thermochemistry, thermochemical kinetics, noncovalent interactions, excited states, and transition elements: Two new functionals and systematic testing of four M06-class functionals and 12 other functionals. *Theor. Chem. Acc.* **2008**, *120*, 215–241.
56. Ditchfield, R.; Hehre, W.J.; Pople, J.A. Self-consistent molecular-orbital methods IX: An extended Gaussian-type basis for molecular-orbital studies of organic molecules. *J. Chem. Phys.* **1971**, *54*, 724–728. [[CrossRef](#)]
57. Hehre, W.J.; Ditchfield, R.; Pople, J.A. Self-consistent molecular orbital methods XII: Further extensions of Gaussian-type basis sets for use in molecular orbital studies of organic molecules. *J. Chem. Phys.* **1972**, *56*, 2257–2261. [[CrossRef](#)]
58. Hariharan, P.C.; Pople, J.A. The influence of polarization functions on molecular orbital hydrogenation energies. *Theor. Chim. Acta* **1973**, *28*, 213–222. [[CrossRef](#)]
59. Hay, P.J.; Wadt, W.R. *Ab-initio* effective core potentials for molecular calculations: Potentials for the transition metal atoms Sc to Hg. *J. Chem. Phys.* **1985**, *82*, 270–283. [[CrossRef](#)]

Disclaimer/Publisher’s Note: The statements, opinions and data contained in all publications are solely those of the individual author(s) and contributor(s) and not of MDPI and/or the editor(s). MDPI and/or the editor(s) disclaim responsibility for any injury to people or property resulting from any ideas, methods, instructions or products referred to in the content.